

Stress transfer by shear in carbon fibre model composites

Part 2 Computer simulation of the fragmentation test

J.-P. FAVRE, P. SIGETY, D. JACQUES

Office National d'Etudes et Recherches Aéronautiques BP 72, 92322-Châtillon Cedex, France

A simulation of the fragmentation process experienced by a single fibre embedded in a resin matrix specimen loaded in tension is presented. The model is based on a combination of two successive regimes of stress building at the fragment extremities, namely elastic stress transfer and friction, and assumes the pull-out strength as the debonding criterion. The computed ultimate fragment length and interfacial transfer shear stress are compared with the experimental results.

1. Introduction

It was established in Part 1 [1] that the interfacial shear stress τ_m that can be calculated from fragmentation tests of a single fibre embedded in a resin tensile specimen is sensitive to the fibre surface treatment in addition to both the resin Young's modulus and the fibre properties. Instead of simply giving the ultimate shear strength as other single fibre tests (pull-out or curved-neck compression specimens) do, the fibre and the matrix are both involved as they actually are in composites but in a rather simplified way, without fibre–fibre interactions. What is tested is thus the ability of the whole system (fibre + matrix + interface) to transfer stresses. Indeed, for fixed fibre and matrix, this ability depends on the interface quality which explains the wide use of the technique for fibre surface treatments or sizings comparison.

Modelizations of the fragmentation process, an intermediate step to the comprehensive description of the unidirectional composite rupture process, have been proposed by Fraser *et al.* [2–4] or Ochiai and Osamura [5, 6].

In Fraser's work, the determination of the interfacial shear strength τ is the result of an optimization procedure intended to put the theoretical and experimental critical aspect ratio distributions in agreement with each other. The theoretical distributions are based upon a stochastic fracture process of the fibre considered as a chain of links with a bimodal strength distribution. Optimization is needed because two parameters are to be evaluated at the same time: the "effective interfacial shear strength" τ which is a measure of the interface ability to transfer stresses and the "distance between severe flaws on the fibre". The latter may change from one fibre treatment to another as fibres are supposed to be more or less protected according to the treatment.

For Fraser, τ is supposed to vary between 0 and the shear yield stress of the matrix, estimated from the tensile properties of the plain matrix using the Von

Mises criterion. According to the Kelly–Tyson shear-lag analysis [7], stress transfer takes place at constant shear stress. No indication is given by the authors of how far the results of the optimization method are when compared with the rough application of the Kelly–Tyson equilibrium equation: the former is more accurate according to DiBenedetto [8].

Miwa *et al.* [11] have the same approach but they always keep the elementary link of their fibre chain longer than the smallest broken fibre piece so that the strength distribution is assumed to be uniform in each fragment when the fragmentation has come to the end. Fitting the theoretical fragment length distribution to the experimental one in the Kelly–Tyson equation where the probability density function $f(\sigma)$ where σ is the fibre stress replaces the fibre strength finally gives τ . As Miwa and Fraser work on glass–thermosets and glass–thermoplastics, respectively, their results cannot be compared.

In a series of six papers on the fracture of metal matrix composites, Ochiai and Osamura gave another version of the multiple fracture process simulation [5, 6]. Again, a random generator is used to attribute the Weibull distributed strengths to the fibre chain divided into a number of elements. In their analysis, several modes of deformation, representative of the metal matrix they are dealing with, are introduced and the interfacial shear strength is assumed to be higher than the shear yield stress of the metal matrix (no debonding). Experimental and simulation data are well matched in terms of the number of fracture sites or average critical ratio as a function of the fibre volume fraction (fibre diameter against coating thickness ratio). In a later work, Ochiai and Osamura applied the same model to metal fibres covered with a brittle fracturing coating; again, no debonding was assumed to occur [9, 10].

The aim of the present paper is to extend the previous simulations to the case of the carbon fibre resin systems of Part 1 [1] with the introduction of some

friction at the fibre-matrix interface once the debonding has occurred. The pull-out strength determined on single fibres has been taken as the criterion for debonding.

2. Basic assumptions

The fibre has been assumed to be linear elastic with a strength that obeys a two-parameter Weibull distribution function. In this first version of the model, the resin matrix was not considered to deform plastically and the Young's modulus is presumed to perfectly describe its properties.

Owing to the pronounced anisotropy of the carbon fibres and the strong thermal mismatch between fibre and resin, the thermal stresses, that give their full effect on the single fibre composite geometry, affect the stress-transfer conditions very significantly, especially when friction is effective. Another consequence is that the fibre is put initially on axial compression so that, when tension is applied, the first failure occurs at a strain which is delayed by a corresponding quantity. Thermal residual stresses have been calculated according to Eshelby [12] for an elastic model.

Two conditions of stress transfer at the interface, namely elastic stress transfer up to the interface failure, then stress transfer by friction, have been combined into a mixed mode. They are all illustrated in Fig. 1.

For elastic stress transfer (Fig. 1a), at low applied loads, the matrix deforms elastically in shear. The Cox expressions [13] of stress equilibrium have been used, giving the following equations for the fibre tensile stress σ and the matrix shear stress τ respectively

$$\sigma(x) = \varepsilon_{\infty} E_f \left(1 - \frac{\cosh \beta(\frac{l}{2} - x)}{\cosh \beta \frac{l}{2}} \right) \quad (1)$$

where ε_{∞} is the specimen deformation, E_f the fibre Young's modulus, x the stress transfer length (elastic) and

$$\beta^2 = \frac{2G_m}{E_f r_f^2 \ln(R/r_f)} \quad (2)$$

where G_m is the matrix shear modulus, r_f the fibre radius, and R the matrix equivalent radius.

$$\tau_e(x) = \varepsilon_{\infty} E_f \frac{r_f}{2} \beta \left(\frac{\sinh \beta(\frac{l}{2} - x)}{\cosh \beta \frac{l}{2}} \right) \quad (3)$$

where τ_e is the elastic shear stress. σ is a maximum for $x = l/2$, where l is the length of the fibre piece. Conversely, τ_e is a maximum for either $x = 0$ or $x = l$ at the fragment ends. Letting x' be the stress transfer length for which the fibre strain differs from ε_{∞} only by a very small quantity δ gives

$$x' = \frac{1}{\beta} \ln \frac{1}{\delta} \quad (4)$$

The stress transfer length x' depends only on the elastic properties and geometrical characteristics of the system.

If there is no bonding at the interface, shear is limited by friction (Fig. 1b) and given by

$$\tau_f = \mu P \quad (5)$$

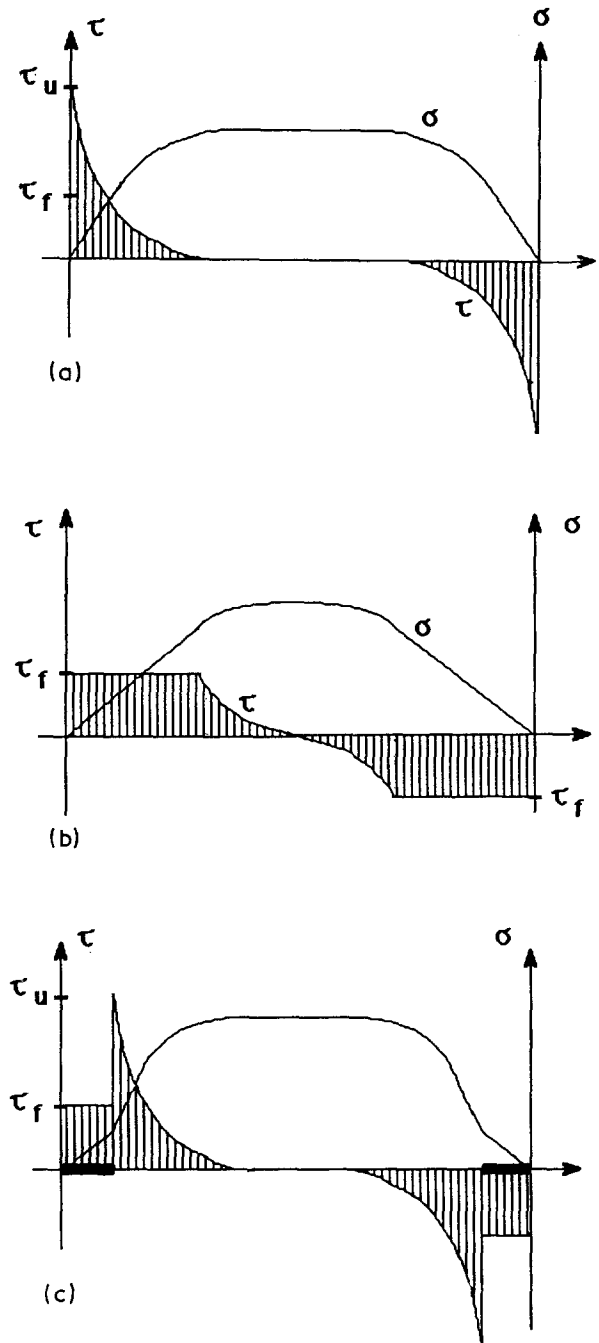


Figure 1 Stress profiles along a fragment: (a) elastic case, (b) friction, (c) combination of modes.

where τ_f is the friction shear stress, μ the coefficient of friction and P the radial pressure on the fibre which depends on the overall deformation of the specimen by the Poisson effect and is calculated by the same equations as the residual thermal stresses [14]. $\sigma(x)$ is given accordingly by integration over the distance x . In the central part of the fragment, where the elastic solution would give $\tau < \tau_f$, elastic stress transfer is recovered. As the Poisson contraction of the fibre decreases linearly with the fibre tensile stress, P is not uniform and τ_f should be highest at the fragment ends. If τ_f is taken as a constant along the fibre has been verified to be within 5% of the expected value.

A combination of the two preceding modes gives the stress profile of Fig. 1c: the elastic stress transfer is limited by the ultimate debonding strength τ_u . At the

fragment ends, where $\tau > \tau_u$, this mode is now replaced by friction with $\tau = \tau_f$. When moving towards the middle of the fragment, elastic stress transfer is recovered as soon as the computed elastic solution gives $\tau_e < \tau_u$. The mean shear stress τ_m is the average value of τ along the half fragment.

This combination of two modes of stress transfer has already been suggested by Piggott [15] who discussed the mechanisms of pull-out of weakly bonded fibres.

Even if not obvious in the representations of Fig. 1, stress transfer may involve the two modes unsymmetrically and the point where $\tau = 0$ may not coincide with the fragment mid-point [14]. The shear profile is calculated for each fragment to satisfy the equilibrium equations and the boundary conditions.

The criterion τ_u is taken as equivalent to the pull-out strength, independently determined from experiments where fibres are extracted from a resin matrix. According to Désarmot *et al.*, leaning on a former analysis of the pull-out by Greszczuk, τ_u is given as the limit of the pull-out strength when the embedded length of fibre tends to zero [16, 17].

3. Computer simulation

The fibre of initial length L_f is divided into n elements of length L_m and average strength $\sigma_R(L_m)$. This strength is determined from the extrapolation down to L_m of the strength against gauge length relationship using the parameters of the Weibull distribution calculated for the fibre. The number of elements is currently 2500, that is $L_m = 4 \mu\text{m}$ for an initial 10 mm long fibre.

To each element $i_1, i_2 \dots i_n$ is affected randomly a strength $\sigma_{R(i)}$ given by

$$\sigma_{R(i)} = \frac{\sigma_R(L_m)}{\Gamma\left(1 + \frac{1}{m}\right)} \left[\ln\left(\frac{1}{1 - R(i)}\right) \right]^{1/m} \quad (6)$$

where σ_R is the fibre rupture strength, m the Weibull shape parameter of the fibre and $R(i)$ a random number giving the link i its strength $\sigma_{R(i)}$. The result is a fibre with a random distribution of flaws and corresponding element strengths.

The fibre is now considered to be surrounded by the matrix with proper residual thermal stresses. Deformation is introduced by increments to the specimen up to the fibre failure at the first critical flaw. For each step of the deformation, the radial pressure on the fibre is calculated. When the fibre fails, and for each new failure at increasing deformations, the elastic solution is first computed taking for zero, on both newly created fibre ends, the transfer length at constant shear stress (no friction). Then

- (i) values of $\tau_e > \tau_f$ in debonded parts are replaced by τ_f ;
- (ii) for values of $\tau_e > \tau_u$ in bonded parts, the transfer length at constant $\tau = \tau_f$ is given an increment.

After each of these steps, the stress state is computed again as many times as the above conditions can be satisfied.

As mentioned before, since the non-symmetry of the fragment stressing mode has to be maintained, the point along the fragment where the shear changes its sign must be found first and the program provides two separate parts to calculate the above solutions on each side of the zero-shear position. Full details on the organigram have been given elsewhere [14].

Once the shear profile has been determined at each step for all fragments, the corresponding fibre tensile stresses are calculated and compared to the actual strength of the remaining unbroken elements. Again,

- (i) if $\sigma > \sigma_{R(i)}$, a new failure occurs and the above procedure is repeated from the very start;
- (ii) if $\sigma < \sigma_{R(i)}$, the program stops and the final values are calculated: mean fragment length l_m , critical fragment length $l_c (= 4 l_m/3)$, strength of the fibre at l_c and, finally, the mean transfer shear stress τ_m .

Typical displays of the results at various times are presented in Fig. 2 for the initial 10 mm long fibre and a 1 mm long detail. The initial unbroken fibre is shown in Fig. 2a: shear due to the axial compressive residual stresses is present only at the extremities of the fibre. In the upper part of the representation of the 10 mm fibre, the "cloud" of the randomly distributed element strengths has been made visible. In Fig. 2b, for some deformation of the specimen, the weakest element has failed and elastic stress transfer takes place on both sides of the broken element.

The final situation when the program has just stopped (no more fibre failure or "saturation" state) is represented in Fig. 2c and d with $\tau_u = 60$ and 130 MPa, respectively. In Fig. 2c, stress transfer has been achieved mainly by friction, with its easily recognizable rectangular shear stress and triangular fibre tensile stress profiles. The fibre is almost completely debonded (black lengths). In Fig. 2d, for a system with a very good fibre-matrix bonding strength, the stress profiles are typical of a combined elastic-friction stress transfer with large (white) lengths where the fibre-matrix bond did not break.

4. Results

4.1. Input values

The relevant input values for the fibre, resin and interface characteristics are summarized in Table I for six fibre-resin systems. All of them have been experimentally determined except for the fibre properties in the transverse direction (Poisson's and thermal expansion coefficients) and the fibre-matrix friction coefficient for which estimations reported in the literature have been used.

The fibre strength distributions were based on data determined according to the procedure described in Part I of the paper and extrapolated down to $4 \mu\text{m}$ (length of one link) using the Weibull transformation expression. For the matrix, R , in Equation 2 is taken as the equivalent radius of the resin specimen reduced to a cylinder.

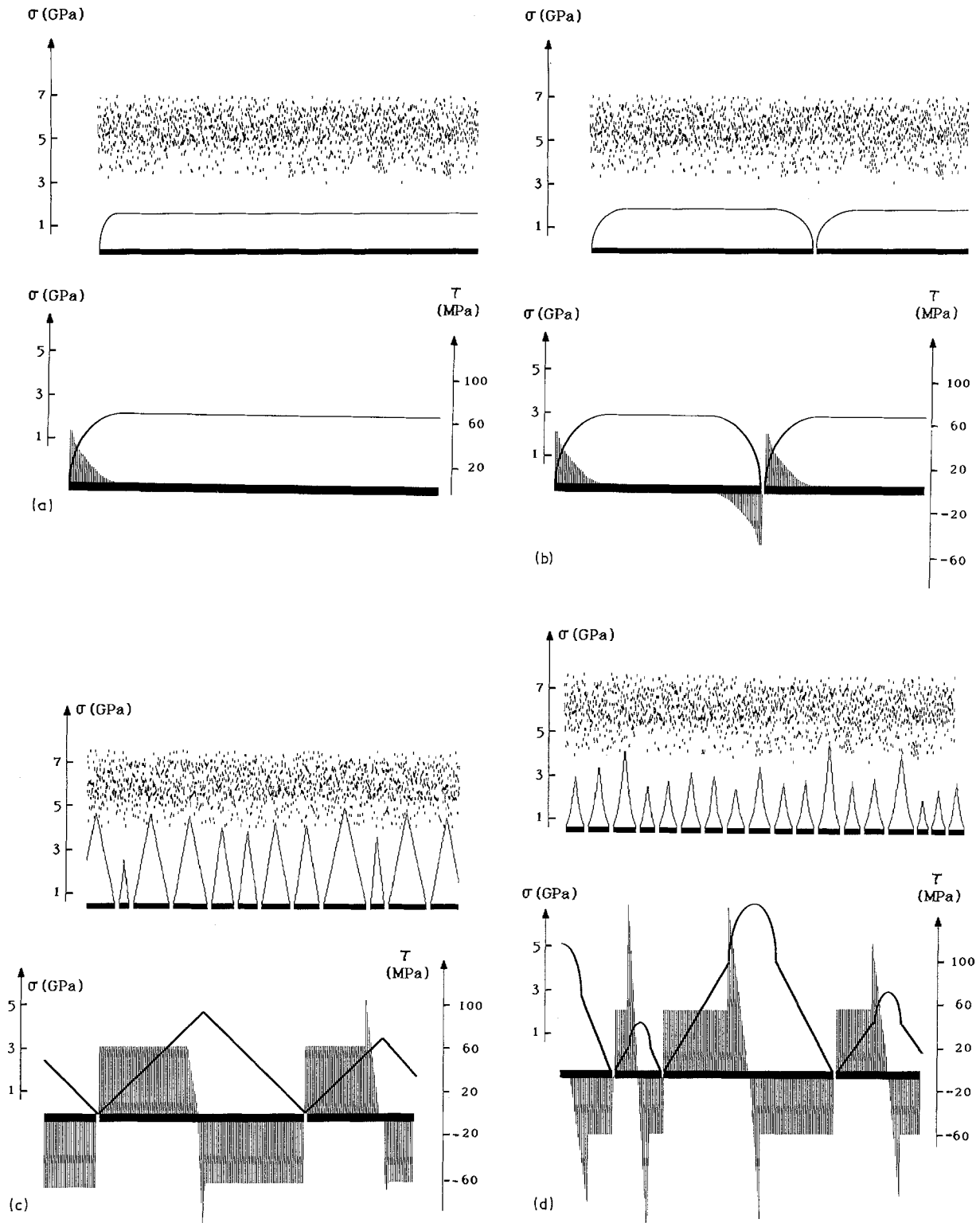


Figure 2 Results of the simulation: (a) initial state, (b) first fibre breakage, (c) final state (weakly bonded system, $\tau_u = 60$ MPa), (d) final state (strongly bonded system, $\tau_u = 130$ MPa).

The fibre–matrix friction coefficient is a matter for discussion. In most carbon–epoxy systems, very high strengths are experienced in the pull-out test; and the elastic energy stored in the free length of fibre is high enough to let the embedded part be extracted suddenly without any control, which prevents the friction coefficient being calculated as Chua and Piggott [15] did for other systems. Based on these authors' data, a constant value of 0.9 was introduced for all systems throughout the present work. As it will be discussed below, the point is of importance for τ_m computation.

4.2. Simulation against experiment comparison

Final results are compared in Table II for the six carbon–resin systems. Experimental values of l_c and τ_m are the average of five tensile specimens. Agreement between both sets of data is observed. As it will be discussed in the next section, τ_{mc} in Table II is more representative of the fragmentation process as the tensile strength of the remaining fibre pieces is continuously recalculated at each step of the program. Since, however, experimentally determined τ_m refers to

TABLE I Materials characteristic input values

	T300	T800	AS4
E_{fL} (GPa)	230	294	220
E_{fT} (GPa)	18	23	18
ν_{fLT}	0.26	0.26	0.26
ν_{fTT}	0.39	0.39	0.39
m	11.5	7.5	4.1
σ_0 (MPa)	3907	7543	4100
r_f (10^{-6} m)	3.50	2.50	3.63
α_{fL} ($10^{-6} \text{ }^\circ\text{C}^{-1}$)	-1	-1	-1
α_{fT} ($10^{-6} \text{ }^\circ\text{C}^{-1}$)	19	19	19
	Araldite LY556	Narmco 5208	Narmco 5245
E_m (GPa)	2.70	3.85	3.95
ν_m	0.45	0.35	0.35
R (10^{-3} m)	2	2	2
α_m ($10^{-6} \text{ }^\circ\text{C}^{-1}$)	55	50	50
T_c ($^\circ\text{C}$)	140	180	180
	τ_u (MPa)		τ_u (MPa)
T300	UT/LY556 60	T800	ST/LY556 50
T300	UT/5208 130	T800	ST/5245 103
T300	ST/5208 150	AS4	ST/LY556 67

L and T refer to the axial and transverse directions respectively f and m refer to the fibre and the matrix respectively
 ν Poisson's ratio
 T_c curing temperature
 σ_0 Weibull scaling factor
 α coefficient of thermal expansion

the tensile strength of the fibre at its final length l_c , there is no alternative but to compare τ_m values.

Together with the interface parameters l_c and τ_m , the specimen deformation at two characteristic stages of the fragmentation process have been tabulated: (i) at the first failure of the fibre, where the differences between the observed rupture strain and that of a fibre out of the matrix are to be attributed to the residual thermal stresses and (ii) at the outset of the debonding. It is quite noteworthy that, with the T800 fibre, debonding occurs as early as the first fibre failure. This is in accordance with both the relatively high strain-to-rupture of the fibre and the relatively weak bonding strength of the T800-resin pairs.

As the difference between the first two columns gives an indication of how early the debonding starts, it follows, when the τ_m s are compared, that friction is not as effective as elastic transfer for the stress to

build-up in the fibre. This is confirmed by the stress profiles and number of broken elements in Fig. 2c and d.

5. Discussion

Owing to the above simulation, the relative influence of the various parameters could be studied thoroughly. This influence is very dependent on the stage of the process that is referred to, namely elastic stress transfer or stress transfer by friction, both regimes being separated by the threshold of the fibre-matrix debonding.

Whenever the elastic transfer takes place, the stress transfer length x' of Equation 4 is a function of $(E_f/G_m)^{1/2}$ when replacing β by its value in Equation 2. The critical length l_c , which is currently computed when the fragmentation has been completed, differs from x' as the fibre strength distribution is now involved in the simulation. Plotting l_c/d as a function of $(E_f/G_m)^{1/2}$ thus gives the line of Fig. 3, which fully supports the previous statements of Galiotis *et al.* [18] for fibres of various diameters or Nardin *et al.* [19] for resins of various moduli respectively. Fig. 3 refers to a fictitious system with $\tau_u = 200$ MPa while elastic stress transfer is limited by debonding in actual systems, cf Table II.

As soon as friction is superimposed to the elastic stress transfer, the effect of changing the matrix modulus becomes more complex. The Fig. 4a and b give typical computed data of τ_m as a function of the Young's modulus of the matrix for $\tau_u = 50$ and 150 MPa respectively and four values of the friction coefficient. Here again, the situations refer to the final state of the fragmentation process. As expected, the effect of changing μ can be made out only whenever debonding has occurred, which happens very early (distinct plots from the very start) for $\tau_u = 50$ MPa but very late (mingled plots up to $E_m = 3$ GPa) for $\tau_u = 150$ MPa. Referring back to Table II, the systems 4 and 3 are representative of these two situations, respectively. That the good agreement observed in Table II may be attributed to a properly selected coefficient of friction should not be ruled out.

Anyway, the present simulation is not completely free of shortcomings, some of them being discussed below.

(i) Once the fibre-matrix interface has failed, the crack is likely not to propagate in a stable way as it

TABLE II Simulation/experience data comparison (l_c in μm ; τ_m in MPa)

System	Simulation						Experience		
	$\epsilon(\%)^a$	$\epsilon(\%)^b$	l_c	τ_m	τ_{mc}	l_c	τ_m		
1	T300	UT/LY556	2.16	2.35	608	25	27	579	24.9
2	T300	UT/5208	2.26	3.60	342	46	53	359	47.6
3	T300	ST/5208	2.40	4.25	289	55	68	300	59.3
4	T800	ST/LY556	2.59	2.59	1128	16	21	1290	14.0
5	T800	ST/5245	2.86	2.86	662	28	33	558	36.3
6	AS4	ST/LY556	—	—	941	18	—	580	51.0

^a first fibre rupture

^b debonding

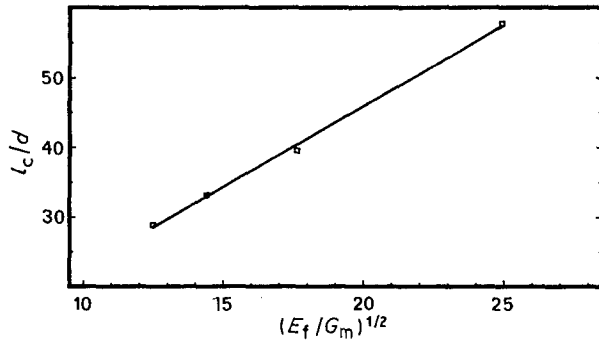


Figure 3 Results of the simulation: influence of the constituents moduli ratio on the critical aspect ratio (strongly bonded system).

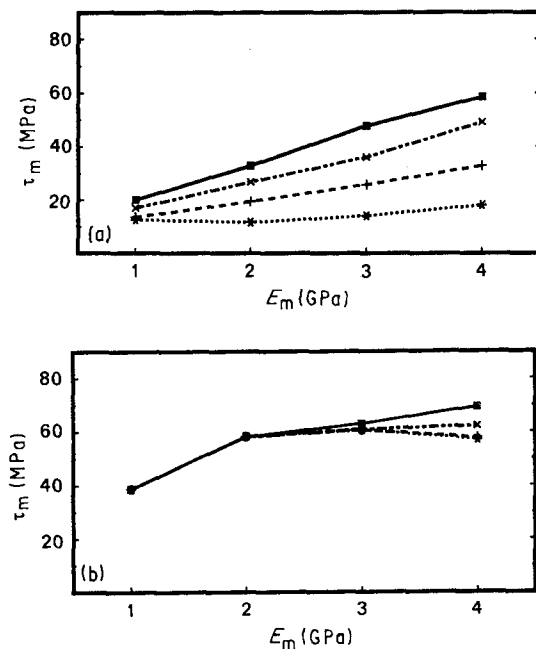


Figure 4 Results of the simulation: effect of the matrix Young modulus on the interfacial transfer shear stress for some values of the friction coefficients: (a) weakly bonded system ($\tau_u = 50$ MPa), (b) strongly bonded system ($\tau_u = 150$ MPa). (■ $\mu = 2$, × $\mu = 1.5$, + $\mu = 1$, * $\mu = 0.5$).

does in the model where links are progressively discharged for each debonding increment, see Section 3. The unstable crack propagation is confirmed by the *in situ* video monitoring of the mechanical test. The penny-shape cracks that form in the matrix normally to the broken fibre are not taken into consideration, but should perturb the stress building at the fragment ends.

(ii) The fibre strength distributions are based on linear extrapolations from experimental measurements at millimetre gauge lengths down to the length of one link by means of the Weibull statistics. That may be an oversimplification of the strength against length relationship. As reported above, that could explain why the simulation fails for fibres of low Weibull modulus (AS4).

(iii) Finally, the viscoelastic properties of the resin matrix are ignored in this version of the model on behalf of Young's modulus only. One of the various implications is that the calculated maximum elastic

shear stress τ_{\max} may possibly exceed the matrix yield shear stress, τ_y determined on plain resin specimens. Indeed, typical values for the most efficient system (T300 ST/5208) are $\tau_u = 150$ MPa while τ_y has been found to be 75 MPa for plain 5208 from rail-shear tests [20]. The various τ s are not, however, on an equal footing as far as fragmentation is concerned: τ_y is associated to the macroscopic properties of a large volume of material while τ_u refers to a small area of fibre surrounded by the resin. Anyway, the significance of τ_u has been discussed elsewhere [17].

On the contrary, with the present model, it is possible to correct for some aspects of the fragmentation process that otherwise would be disregarded: in the multiple rupture process, the fibre breaks progressively and the strength of the remaining fibre pieces continuously increases (volume effects as well as elimination of the most critical flaws) whereas, to calculate the final τ_m , experiments make use of the fibre tensile strength originally determined once for all from tensile tests at various gauge lengths. A systematic bias is thus introduced in the experimental values of τ_m .

A second bias is related to the stress profile along the fragments: the most critical flaw may be located in the ascending part of the stress profile and thus, in a way, protected against failure which eventually occurs at the maximum stress on a less critical flaw.

Allowance is made for both deviations in the computer simulation, giving the τ_{mc} values, while it cannot be in the experimental based τ_m determinations. Both have been indicated in Table II.

Acknowledgements

This work, forming a part of the PhD Thesis of D. Jacques, was partly funded by a grant of FIMAC.

References

1. J.-P. FAVRE and D. JACQUES, *J. Mater. Sci.* **25** (1990) 1373–1380.
2. W. A. FRASER, F. H. ANCKER and A. T. DIBENEDETTO, 30th Annual Technology Conference 1975, Reinforced Plastics/Composites Institute, The Society of the Plastics Ind., Inc., section 22A.
3. W. A. FRASER, F. H. ANCKER, A. T. DIBENEDETTO and B. ELBIRLI, *Polym. Compos.* **4** (1983) 238–248.
4. A. T. DIBENEDETTO, L. NICOLAIS, L. AMBROSIO and J. GROEGER, in "Composite Interfaces", edited by H. Ishida and J. L. Koenig (Elsevier Science, Amsterdam, 1986) p. 47.
5. S. OCHIAI and K. OSAMURA, *Z. Metallk.* **77** (1986) 255–259.
6. S. OCHIAI and K. OSAMURA, *Z. Metallk.* **77** (1986) 249–254.
7. A. KELLY and W. R. TYSON, *J. Mech. Phys. Solids* **13** (1965) 329–350.
8. A. T. DIBENEDETTO, *Pure Appl. Chem.* **57** (1985) 1659–1665.
9. S. OCHIAI and K. OSAMURA, *J. Mater. Sci.* **21** (1986) 2735–2743.
10. *Idem.*, *ibid.* **21** (1986) 2744–2752.
11. M. MIWA, T. OHSAWA and K. TAHARA, *J. Appl. Polym. Sci.* **25** (1980) 795–807.
12. J. D. ESHELBY, in "Progress in Solid Mechanics" Vol. 2 (Suedden & Hill, Amsterdam, 1961).
13. H. L. COX, *Brit. J. Appl. Phys.* **3** (1952) 72–79.

14. D. JACQUES, PhD Thesis, Institut National Polytechnique de Lorraine (1989).
15. M. R. PIGGOTT, A. SANADI, P. S. CHUA and D. ANDISON, in "Composite Interfaces", edited by H. Ishida and J. L. Koenig (Elsevier Science, Amsterdam, 1986) p. 109.
16. G. DÉARMOT and M. SANCHEZ, "Quatrièmes Journées Nationales sur les Composites (JNC-4)", edited by G. Verchery (Pluralis, Paris, 1984) p. 449.
17. M.-F. MARMONIER, G. DÉARMOT, B. BARBIER and J.-M. LETALENET, *J. Mécanique théorique appliquée* 7 (1988) 741–765.
18. C. GALIOTIS, R. J. YOUNG, P. H. J. YEUNG and D. N. BATCHELDER, *J. Mater. Sci.* 19 (1984) 3640–3648.
19. M. NARDIN, E. M. ASLOUN and J. SCHULTZ, "Sixièmes Journées Nationales sur les Composites (JNC-6)", edited by J.-P. Favre and D. Valentin (AMAC, Paris, 1988) p. 157.
20. C. G'SELL, D. JACQUES and J.-P. FAVRE, *J. Mater. Sci.*

*Received 17 August 1989
and accepted 19 February 1990*